REPORT DOCUMENTATION PAGE

Form Approved
OMB NO. 0704-0188

1. AGENCY USE ONLY (Leave Blank)	2. REPORT DATE 6/15/03	3. REPORT TYPE AND DATES COVERED Final– 15 Sep 99 – 14 Jun 03

4. TITLE AND SUBTITLE
Research on Magnetoinductive NDE Techniques to Measure Tensile Strength and Fracture Toughness in Steels as They are Manufactured

5. FUNDING NUMBERS
DAAD19-99-C-0041

6. AUTHOR(S)
Martin J. Sablik and Gary L. Burkhardt

7. PERFORMING ORGANIZATION NAME(S) AND ADDRESS(ES)
Southwest Research Institute
P.O. Drawer 28510
6220 Culebra Road
San Antonio, TX 78228-0510

8. PERFORMING ORGANIZATION REPORT NUMBER 5

9. SPONSORING / MONITORING AGENCY NAME(S) AND ADDRESS(ES)
U. S. Army Research Office
P.O. Box 12211
Research Triangle Park, NC 27709-2211

10. SPONSORING / MONITORING AGENCY REPORT NUMBER
40178.6-MS

11. SUPPLEMENTARY NOTES
The views, opinions and/or findings contained in this report are those of the author(s) and should not be construed as an official Department of the Army position, policy or decision, unless so designated by other documentation.

12 a. DISTRIBUTION / AVAILABILITY STATEMENT

Approved for public release; distribution unlimited.

12 b. DISTRIBUTION CODE

13. ABSTRACT (Maximum 200 words)

The project was (1) to investigate the interrelationship between mechanical properties and magnetic properties by developing an understanding of how microstructure interconnects the two properties and (2) to test if nonlinear harmonics of the magnetic induction could be used to nondestructively determine tensile strength and fracture toughness. The project has been (1) the first to show, via magnetic hysteresis modeling, how inverse grain size and dislocation density affect the parameters controlling magnetic hysteresis; (2) the first to show that with coils wrapped around the specimen, harmonic amplitudes decrease with increasing dislocation density and inverse grain size, and hence with increasing tensile strength; (3) the first to distinguish important differences in microstructural dependences of magnetic properties between hysteresis loops of the same maximum field intensity H_{max} and hysteresis loops of the same maximum magnetic induction B_{max}; and (4) the first to investigate whether or not correlative relationships exist between NLH and fracture toughness. In technology transfer, a pilot program was set up under a separate program to test the use of NLH to nondestructively monitor tensile strength in moving steel sheet in a German steel plant.

14. SUBJECT TERMS
magnetic properties, nonlinear harmonic amplitudes, NLH, tensile strength, grain size, dislocation density, steels, fracture toughness

15. NUMBER OF PAGES
11

16. PRICE CODE

17. SECURITY CLASSIFICATION OR REPORT	18. SECURITY CLASSIFICATION ON THIS PAGE	19. SECURITY CLASSIFICATION OF ABSTRACT	20. LIMITATION OF ABSTRACT
UNCLASSIFIED	**UNCLASSIFIED**	**UNCLASSIFIED**	**UL**

RESEARCH ON MAGNETOINDUCTIVE NDE TECHNIQUES TO MEASURE TENSILE STRENGTH AND FRACTURE TOUGHNESS IN STEELS AS THEY ARE MANUFACTURED

FINAL REPORT

ARO Project No. DAAD19-99-C-0041
SwRI Project No. 14.03198

Prepared for

U.S. Army Research Office
P.O. Box 12211
Research Triangle Park, NC 237709-2211

Prepared by

M. J. Sablik and G. L. Burkhardt
Southwest Research Institute®
San Antonio, TX 78228-0510

June 2003

SOUTHWEST RESEARCH INSTITUTE
SAN ANTONIO **HOUSTON**
DETROIT **WASHINGTON, DC**

TABLE OF CONTENTS

LIST OF TABLES, ILLUSTRATIONS AND APPENDICES

TABLES: Page

FIGURES:

APPENDICES:

I. STATEMENT OF THE PROBLEM STUDIED

Since the Army is interested in techniques of producing stronger steels, more resistant to fracture, for military use and since the conventional methods of testing steels for strength and fracture toughness are destructive in nature, it was proposed that this project be a fundamental study to understand whether mechanical properties can be correlated with magnetic properties, and if so, to understand how and why this happens and how the interrelationship is connected with the underlying microstructure. Because harmonics of the magnetic induction are easily measured, a specific interest was to test if such harmonics could be used to nondestructively measure tensile strength and fracture toughness in steel.

Thus the project was (1) to investigate the interrelationship between mechanical properties and magnetic properties by developing an understanding of how microstructure interconnects the two properties and (2) to test if nonlinear harmonics of the magnetic induction could be used to nondestructively determine tensile strength and fracture toughness, and if so, how and why.

II. SUMMARY OF RESULTS

A. Effect of Tensile Strength on Magnetic Properties and on Nonlinear Harmonic (NLH) Amplitudes

Work in this project used magnetic hysteresis modeling to explain how hysteretic magnetic properties are correlatable with tensile strength. It was known [1] that increasing tensile strength is correlated with decreasing grain size and increasing dislocation density. Certain parameters in magnetic hysteresis model of Sablik and Jiles [2–4] were thus modified to include the contributions of grain size (average grain diameter) and dislocation density. Using appropriate functional dependences of these parameters on grain size and dislocation density, a computer study was then done to investigate how these attributes affected the prediction of magnetic properties like coercivity, remanence, maximum differential permeability, and hysteresis loss. In the range of grain sizes and dislocation densities found in already measured specimens [5], the computed coercivity was found to show a linear dependence on inverse grain size and a proportionality with the square root of dislocation density, just as found experimentally. The remanence and maximum differential permeability, on the other hand, decreased with respect to inverse grain size and square root of dislocation density. The hysteresis loss showed increase with increasing inverse grain size and square root of dislocation density, in agreement with experiment, but outside the range tested experimentally, it showed opposite tendencies at very small grain size and large dislocation density, showing the effect of being dominated by remanent behavior instead of coercive behavior. These results were reported in [5,6].

Modeling previously developed [7] for computing the first and third harmonic amplitudes was modified to investigate the effect of grain size and dislocation density on the first and third harmonic amplitudes of the magnetic induction. It was found that the computed harmonic amplitudes decreased with decreasing grain size and increasing dislocation density. Since decreasing grain size and increasing dislocation density correlate with increasing tensile strength, in effect it was found that the harmonic amplitudes decreased with increasing tensile strength, as shown experimentally by the experimenters at IKPH at the University of Hannover in Germany.

Finally, the modeling of the harmonic amplitudes was extended to higher frequencies, taking into account classical eddy current power loss and excess power loss [8]. The higher frequency model of Jiles [9] was modified to include the effects of grain size and dislocation density. A numerical solution of the equations had to be employed. The results [7] agreed with the experimental observation that at a fixed frequency, the harmonic amplitudes decreased with increasing tensile strength. This was seen for specimens with coils wrapped around the specimens themselves. In addition, the prediction was that the harmonic amplitudes were smaller at higher frequencies and that excess loss diminished the amplitudes slightly more. The decrease of the harmonic amplitudes with increasing frequency was seen experimentally. Experiments affirming this behavior were done earlier at the University of Hannover [10].

In this project, experiments were also done with steel sheets and air coils at the University of Hannover in Germany. A large number of separate specimen sheets were tested with respect to the correlation between harmonic amplitudes and tensile strength. The tested range of tensile strength was extended, and measurements were done at different frequencies. With coils out in the air above and below the sheets, an unusual feature observed was that the third harmonic amplitudes, in the secondary air coils, increased instead of decreased with increasing tensile strength. This differed from the prediction for the third harmonic amplitudes found inside a specimen, and hence this effect with air coil configurations had to be further investigated. The effect of sheet thickness on the measurements was investigated. It was found that amplitudes decreased with increasing thickness for 147 Hz, and for higher harmonics, it was found that the amplitudes decreased more sharply and then leveled off. At higher frequencies (>1400 Hz), the harmonic amplitudes stayed approximately constant with increasing thickness. This is consistent with the expectation that at higher frequencies, there is little penetration of the signal into the material, so the amplitude changes little as thickness is further increased. At lower frequencies, the signal can penetrate the sample volume much more, and the response depends on the volume percentage of sample penetrated. It was also observed that tensile strength had little effect on the thickness dependence.

Meanwhile, an opportunity developed for a collaboration with Luc Dupre of Ghent University in Ghent, Belgium, to extend our predictions of microstructural effects on magnetization to the predictions of the microstructural dependence of Preisach parameters used to fit hysteresis loops by what is known as Preisach hysteresis modeling. Usually, the Preisach model is used to predict hysteresis loops based on fitting sequences of experimental inner hysteresis loops until the final experimental saturation hysteresis loop is reached. In steels, as part of the fitting process, a Lorentzian Preisach distribution function is used to do this. Dupre had studied the Lorentzian Preisach distribution functions needed to fit the experimental hysteresis curves of a family of steel specimens of different grain sizes and had determined how the various Lorentzian Preisach distribution parameters varied with grain size [11]. In a new approach to the modeling, hysteresis curves of inner and saturation loops were obtained using the Jiles-Atherton-like [12] approach that had been used in this project. Hysteresis loops were computed first for a set of different grain sizes and constant dislocation density, and then for a set of different dislocation densities and constant grain size. The first set of loops, involving different grain sizes, was fitted using a Lorentzian Preisach distribution function. Results exhibited good agreement with the earlier fit by Dupre [11] to experimentally obtained loops for different grain sizes. The other set of computed loops, for varying dislocation densities, was used to predict how the Lorentzian Preisach distribution parameters would behave for a new set of experimental specimens with

varying dislocation density and constant grain size. These calculations are now available for future experimental tests. Physical arguments given in our published paper [13] offer explanations as to why the Preisach parameters behave the way they do.

Through conference discussion, it was found that there existed unpublished data for hysteresis loss conflicting with predictions of our model in the case of very small grain size and large dislocation density. F. J. G. Landgraf, in the same conference discussion, suggested what might be responsible for the apparent conflict. He noted that hysteresis loss experimenters compare hysteresis loops of the same maximum flux density B_{max} whereas in our modeling, hysteresis loops of the same maximum magnetic field H_{max} were being compared. The computer program was thus restructured to output hysteresis loops all with the same maximum flux density. This time, predicted hysteresis loss revealed a linear increase with increasing inverse grain size and increasing square root of dislocation density, just as found experimentally for very small grain and large dislocation density. So, the model does indeed reproduce the experimental dependencies. Remanent field behavior in this case does not influence hysteresis loss away from the pattern followed by coercive field behavior because the remanent field remains essentially constant for all loops of the same maximum flux density. Two papers were prepared discussing these effects [14,15]. Also discussed in these papers is the effect of uniaxial microcrystalline anisotropy on the microstructural dependence of the magnetic properties. One byproduct of these new papers is a mathematical argument justifying microstructural interrelationships among the Jiles-Atherton hysteresis parameters found earlier.

Earlier we had discussed results indicating that with primary and secondary coils wrapped around the specimen, the nonlinear harmonic (NLH) amplitudes of the magnetic induction decreased with increasing tensile strength. We have now determined by finite element modeling (See Section C) that the configuration to be used in a steel plant shows somewhat different behavior. For the steel plant, air coils (primary and secondary) are to be used above and below a moving steel sheet. The secondary coil voltage, however, is a measure of the flux density in the air, and not in the specimen itself. The flux density in the air is modified by the presence of the steel sheet, but in the secondary air coils, harmonics change somewhat differently from the flux density harmonics that would be measured in the specimen itself. For the air coils, the third harmonic amplitude monotonically increases with increasing tensile strength, and other harmonics show mixed behavior, with initial decrease and then increase. A way to look at this is to realize that with flux concentrated in the specimen, it gets more difficult to change the flux in the specimen with increasing tensile strength and increasing coercivity, and thus the air coils tend to drive mostly flux changes in the air, which are more easily driven, and hence the higher harmonics increase at the higher tensile strengths.

B. Effect of Fracture Toughness on Nonlinear Harmonic Amplitudes

Because of the retirement of co-P.I. Dieter Stegemann, work at Hannover was concluded in June 2001, and it fell to new co-P.I. Gary Burkhardt at SwRI, who is experienced at nonlinear harmonic (NLH) nondestructive evaluation (NDE) [16,17], to continue experimental work, this time investigating the effect of changing fracture toughness on the harmonic amplitudes.

Experimentally, it was decided that the NLH measurements would be conducted on Charpy specimens since the Charpy test is one way of measuring fracture toughness. Fracture

toughness was varied by heat-treating the specimens prior to testing, according to standard procedures. In setting up such procedures, we have been guided by one of the metallurgists at SwRI, N. S. Cheruvu. Experiments were carried out on two different types of steel, namely 4340 and 9-4-30 steel. Once heat treatments were carried out, the specimens were machined with V-notches, according to the standard Charpy dimensional specifications [18], and then NLH measurements were performed at two separate frequencies for each specimen. Finally, the destructive Charpy tests were carried out and yield strength was measured. In doing the standard Charpy measurements, a knife edge pendulum was dropped from a height h. The minimum height from which the specimen fractures gives a measure of the fracture energy, mgh. Specimens fractured at different temperatures fracture with different fracture energies. The fracture energy vs. temperature curve has a step-like shape, going from a lower brittle fracture energy to a higher ductile fracture energy, known as the upper shelf energy CVN. Different heat treatments shift the mean temperature at which the step occurs, and also different CVN obtain for different specimens. A relationship exists between CVN, the yield strength σ_y, and stress intensity factor K_{1c}, which is often taken as a measure of fracture toughness. The relationship is the following [19]:

$$\left(K_{1c}\right)^2 \Big/ \left(\sigma_y\right)^2 = \left(5/\sigma_y\right)\left\{CVN - \left(\sigma_y/20\right)\right\} \tag{1}$$

In this relationship, σ_y is in ksi, CVN is in ft-lb, and K_{1c} is in ksi $\sqrt{\text{in}}$. We have used this relationship to compute K_{1c}. However the Charpy curves for fracture energy vs. temperature for each specimen often had different temperatures for the beginning of the upper shelf compared to the upper shelf of the curve for % ductile fracture vs. temperature. Thus it was not clear as to where to position the upper shelf and how to compute the CVN. We took a simple estimate and designated the fracture energy at room temperature to be the CVN. Clearly, there are errors in such an estimate. We present two tables. In Table 1, we show the tempering temperature, target hardness, measured hardness, and range of K_{1c} expected for 4340 steel specimens at the indicated tempering temperatures. In Table 2, we show for each 4340 and 9-4-30 specimen the estimated CVN, the measured σ_y, and the computed K_{1c} (averaged over two specimens for each specimen type). Figures 1 and 2 display the dependence of the third and fifth harmonics for each K_{1c} for the two different specimen types, with 150-Hz signal applying to Figure 1 and 1500 Hz applying to Figure 2. Clearly, our results do not indicate a correlative relationship between NLH amplitude and K_{1c} for 150 Hz, and indicate only at most a weak correlation between NLH amplitude and K_{1c} for 1500 Hz. Since the K_{1c} values that we have used are probably in error, it is clear that a more acceptable approach would be to measure K_{1c} directly by a more standard measuring technique [20].

In examining the microstructural features that contribute to fracture toughness, a good correlation between fracture toughness and microstructural features was not obtainable also with the modeling, at least as yet. It so far appears that different features contribute conflicting effects. So the inconclusive correlation obtained experimentally between fracture toughness and NLH amplitude may exist even with better measurement of K_{1c}. Our retired co-PI has recently also done some measurements to explore potential correlation between NLH and fracture toughness properties, and he too has found inconclusive correlation [21]. Thus, it may well be that, although NLH gives good correlation between tensile strength and NLH amplitude (even in the case of air coils, where trends differ from that obtained with wrap-around coils), NLH may not be a good tool for NDE evaluation of fracture toughness. More work is needed to establish this.

Table 1. Information about Sample Preparation for 4340 Steel

4340 STEEL				
Other Info	Tempering Temp	Target Hardness	Actual Hardness	Range K_{1c} from Handbook
4-1	180	58	59.2	23-43
4-2	450	52	54	40-60
4-3	750	47	44.2	70-90
4-4	950	40	38.7	80-130
4-5	1150	33	34.4	90-150

Table 2. Computation of K_{1c} for Both Steels

4340 STEEL						
Specimen	CVN_{est} (ft.lb)	σ_y (ksi)	$\left[CVN_{est} - \frac{\sigma_y}{20}\right]$	$\left[\left(\frac{K_{1c}}{\sigma_y}\right)^2 = \frac{5}{\sigma_y}\left(CVN_{est}\frac{-\sigma_y}{20}\right)\right]$	K_{1c} $\left[\left(ksi\sqrt{in}\right)\right]$	
4-2	17	223	5.85	0.131	80.8	avg
		229	5.55	0.121	79.7	80.3
4-3	14.5	206.5	4.175	0.102	66.0	avg
		199.4	4.53	0.114	67.2	66.6
4-4	31.5	166.2	23.2	0.698	138.8	avg
		178.4	22.6	0.633	141.9	140.4
4.5	70	121.9	63.9	2.62	197.4	avg
		135.3	63.2	2.34	206.8	202.1
9-4-30 STEEL						
9-1	25	211	14.5	0.342	123.5	avg
		211	14.5	0.342	123.5	123.5
9-2	36	205.5	25.7	0.626	162.5	avg
		201.4	25.9	0.643	161.5	162.0
9-3	24	191	14.5	0.379	117.5	avg
		194	14.3	0.355	120.0	118.7
9-4	32	202	21.9	0.542	148.7	avg
		202	21.9	0.542	148.7	148.7
9-5	71	111	65.5	2.95	190.6	avg
		120	65.0	2.71	197.5	194.0

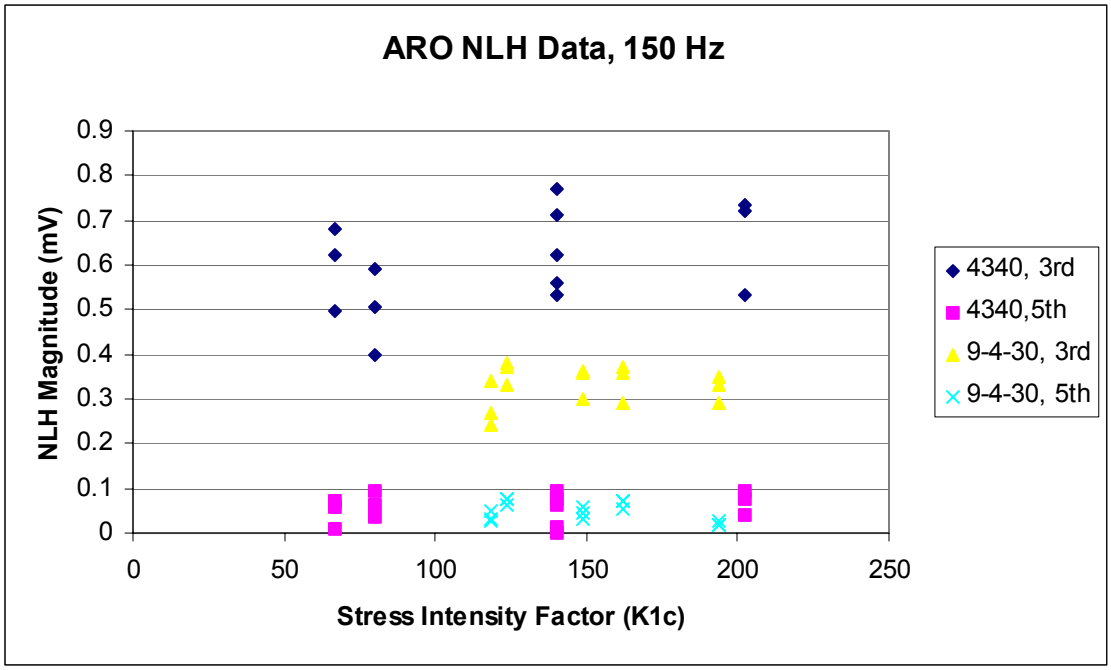

Figure 1. Third and fifth harmonic amplitudes vs. K_{1c} for 4340 steel and 9-4-30 steel for 150-Hz signal

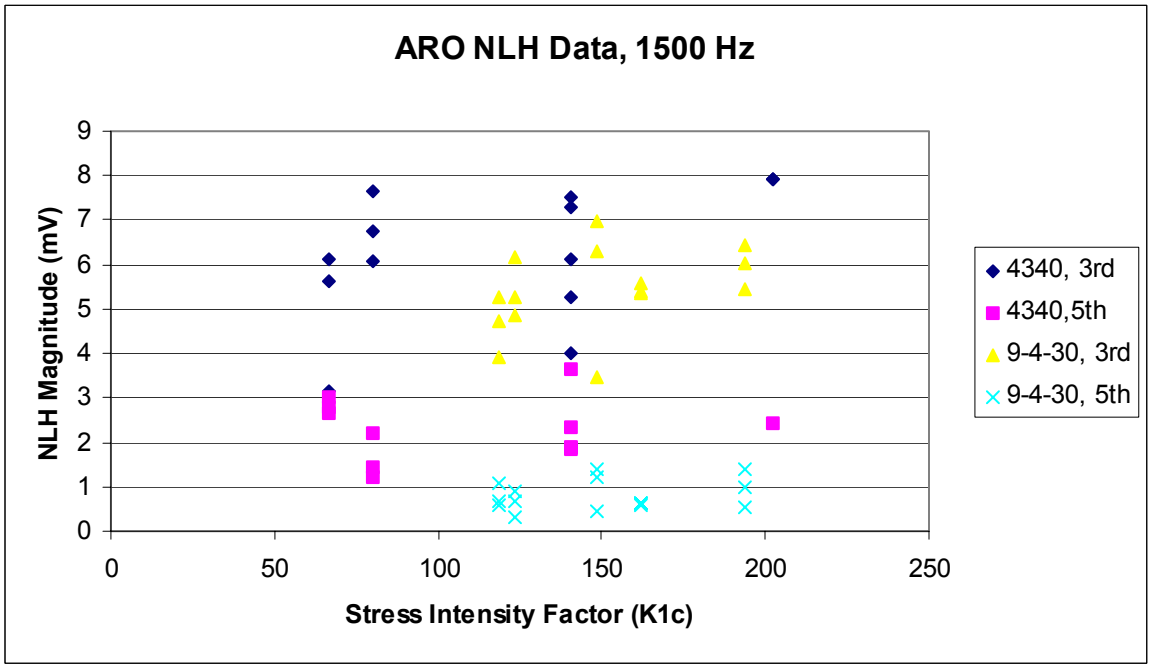

Figure 2. Third and fifth harmonic amplitudes vs. K_{1c} for 4340 steel and 9-4-30 steel for 1500-Hz signal

C. Technology Transfer

As mentioned in our interim reports, the technical group at the University of Hannover has had additional support from the German steel industry (namely, Salzgitter AG) to develop pilot instrumentation to be used on-line in the factory to test sheet steel for its mechanical properties—in particular, tensile strength. An air coil configuration has been built for this purpose and is being tested at the steel plant.

A separate European Union subcontract was issued to SwRI to use finite element modeling and the magnetic model developed for tensile strength effects to unravel the physics of what happens with a complicated coil configuration and to help optimize the coil design. Thus the present ARO project has resulted in additional work, which should bring about better technology transfer.

Another application has been to develop a magnetic test for determining whether a weld is annealed [22]. The modeling on grain size effects and dislocation density effects on magnetization was used as input into a finite element calculation predicting magnetic signal changes as a probe is moved across the various regions of a weld—base metal (away from the weld), heat-affected zone (which exhibits increasing grain size and increasing dislocation density as one moves toward the weld center), and finally the fusion zone in the central part of the weld with large grain sizes, but also large dislocation densities if the weld is unannealed. It turns out that the dislocation density effect dominates the grain size effect when the weld is unannealed, and the permeability (determined from the magnetic signal) decreases sizably as one moves from the base metal to the central part of the weld. On the other hand, when the weld is annealed, dislocation densities greatly decrease, and thus the grain size effect dominates the dislocation density effect, and the permeability actually increases slightly or moderately as one moves from the base metal to the central part of the weld. The two different behaviors tell you immediately whether the weld is annealed or not. This then is an example of how the basic physics exposed by this project can be utilized to design an eminently usable NDE test involving weld characteristics in steels, and thus points to yet another technology transfer application.

REPORT DOCUMENTATION PAGE (SF298)
(Continuation Sheet)

III. PUBLICATIONS AND TECHNICAL REPORTS UNDER THIS CONTRACT

(1) Papers published in peer-reviewed journals:

(a) M. J. Sablik, "Modeling the effect of grain size and dislocation density on hysteretic magnetic properties in steels," *Journal of Applied Physics* **89** (10)**,** pp. 5610–5613 (2001).

(b) M. J. Sablik, D. Stegemann, and A. Krys , "Modeling grain size and dislocation density effects on harmonics of the magnetic induction," *Journal of Applied Physics* **89** (11), pp. 7254–7256 (2001).

(c) L. R. Dupre, M. J. Sablik, R. Van Keer, and J. Melkebeek, "Modeling microstructural effects on magnetic hysteresis properties," *J. Phys. D* **35** (17), 2086 (2003).

(2) Papers presented at meetings, but not published:

(a) M. J. Sablik, "Effect of grain size and dislocation density on magnetic properties and application to monitoring of tensile strength and NDE of welds," invited presentation at the 21st Annual Conference on Properties and Applications of Magnetic Materials (PAMM), Chicago, IL, May 13–15, 2002.

(3) Manuscripts submitted but not published:

(a) M. J. Sablik and F. J. G. Landgraf, "Comparing grain size and dislocation density effects for hysteresis loops with the same maximum flux density in a magnetic hysteresis model," submitted to *J. Appl. Phys.*

(b) M. J. Sablik and F. J. G. Landgraf, "Modeling microstructural effects on hysteresis loops with the same magnetic flux density," accepted by *IEEE Trans. Magn.*

(4) Technical reports submitted to ARO:

(a) M. J. Sablik and D. Stegemann, Interim Report 1 (Sept 1999–Dec 1999).

(b) M. J. Sablik and D. Stegemann, Interim Report 2 (Jan 2000–Dec 2000).

(c) M. J. Sablik and G. L. Burkhardt, Interim Report 3 (Jan 2001–Dec 2001).

(d) M. J. Sablik and G. L. Burkhardt. Interim Report 4 (Jan 2002–Dec 2002).

Note that copies of papers and manuscripts in Parts III (1)-(3) are found in the interim reports, except that (3b) is attached as Appendix A in this report.

IV. SCIENTIFIC PERSONNEL SUPPORTED (in part):

(a) M. J. Sablik, Ph.D., Staff Scientist, Sensor Systems and NDE Technology Department, Applied Physics Division, Southwest Research Institute, San Antonio, TX 78228-0510 (1999–present).

(b) Gary L. Burkhardt, Staff Scientist, Sensor Systems and NDE Technology Department, Applied Physics Division, Southwest Research Institute, San Antonio, TX 78228-0510 (2001–present).

(c) Narayana S. Cheruvu, Staff Engineer, Department of Materials Engineering, Mechanical and Materials Engineering Division, Southwest Research Institute, San Antonio, TX 78228-0510 (2001-present).

(d) Dieter Stegemann, Ph.D., Professor (now retired), University of Hannover, and Director of the Institute of Nuclear Engineering and Nondestructive Testing (IKPH), Hannover, Germany (1999–2001).

(e) Andreas Krys, doctoral student, University of Hannover, Hannover, Germany (2000-2001).

V. INVENTIONS RESULTING FROM PROJECT:

None.

VI. BIBLIOGRAPHY

1. R. W. K. Honeycombe and H. K. D. H. Bhadeshia, *Steels: Microstructure and Properties* (Wiley, NY, 1996), pp. 13–29, 107–113, 221–248.

2. M. J. Sablik and D. C. Jiles, "Coupled Magnetoelastic Theory of Magnetic and Magnetostrictive Hysteresis," *IEEE Trans. Magn.* **29,** 2113 (1993).

3. M. J. Sablik, "Hysteresis Modeling of the Effects of Stress on Magnetic Properties and Its Application to Barkhausen NDE," *Current Topics in Magnetics Research* **1**, 45 (1994).

4. M. J. Sablik, "A Model for Asymmetry in Magnetic Property Behavior Under Tensile and Compressive Stress in Steel," *IEEE Trans. Magn.* **33,** 3958 (1997).

5. M. J. Sablik, "Modeling the Effect of Grain Size and Dislocation Density on Hysteretic Magnetic Properties in Steels," *J. Appl. Phys.* **89**, 5610 (2001).

6. M. J. Sablik, "Effect of Grain Size and Dislocation Density on Magnetic Properties and Application to NDE Monitoring of Tensile Strength and NDE of Welds," presented at the 21st Annual Conference on Properties and Applications of Magnetic Materials (PAMM), Chicago, IL, May 13–15, 2002.

7. M. J. Sablik, D. Stegemann and A. Krys, "Modeling Grain Size and Dislocation Density Effects on Harmonics of the Magnetic Induction," *J. Appl. Phys.* **89**, 7254 (2001).

8. G. Bertotti, "Physical Interpretation of Eddy Current Losses in Ferromagnetic Materials," *J. Appl. Phys.* **67**, 2110 (1985); **67**, 2118 (1985).

9. D. C. Jiles, "Frequency Dependence of Hysteresis Curves in Conducting Magnetic Materials," *J. Appl. Phys.* **76,** 5849 (1994).

10. D. Stegemann, W. Reimche, K. L. Feiste, and B. Heutling, "Determination of Mechanical Properties of Steel Sheet by Electromagnetic Techniques," 8th International Symposium on Nondestructive Characterization of Materials, Boulder, CO, June 1997.

11. L. R. Dupre, G. Ban, M. von Rauch, and J. Melkebeek, "Relation between the Microstructural Properties of Electrical Steels and the Preisach Modeling," *J. Magn. Magn. Mater.* **195**, 233 (1999).

12. D. C. Jiles and D. L. Atherton, "Theory of Ferromagnetic Hysteresis," *J. Magn. Magn. Mater.* **61,** 48 (1986).

13. L. R. Dupre, M. J. Sablik, R. Van Keer, and J. Melkebeek, "Modeling Microstructural Effects on Magnetic Hysteresis Properties," *J. Phys. D* **35** (17), 2086 (2003).

14. M. J. Sablik and F. J. G. Landgraf, "Comparing Grain Size and Dislocation Density Effects for Hysteresis Loops with the Same Maximum Flux Density in a Magnetic Hysteresis Model," submitted to *J. Appl. Phys.*

15. M. J. Sablik and F. J. G. Landgraf, "Modeling Microstructural Effects on Hysteresis Loops with the Same Magnetic Flux Density," accepted by *IEEE Trans. Magn.*

16. H. Kwun and G. L. Burkhardt, "Nondestructive Measurement of Stress in Ferromagnetic Steels Using Harmonic Analysis of Induced Voltage," *NDT International* **20**, 167 (1987).

17. G. L. Burkhardt and H. Kwun, "Application of the Nonlinear Harmonics Method to Continuous Measurement of Stress in Railroad Rail," *Review of Progress in Quantitative NDE,* eds. D. O. Thompson and D. L. Chimenti (Plenum, NY, 1987), Vol.7, pp. 727–735.

18. ASTM E23-01, "Standard Test Methods for Notched Bar Impact Testing of Metallic Materials," *2001 Annual Book of ASTM Standards.*

19. S. T. Rolfe and S. R. Novak, "Slow Bend K_{1c} Testing of Medium Strength, High Toughness Steel," *ASTM STP* **453,** 124 (1970).

20. W. A. Logsdon and J. A. Begley, "Upper Shelf Temperature Dependence of Fracture toughness for Four Low to Intermediate Strength Ferritic Steels," *Engineering Fracture Mechanics* **9**, 460 (1977).

21. D. H. Stegemann, "RPV Material Characterization by Magnetoinductive Method," presented at 3rd International Conference on NDE in Relation to Structural Damage for Nuclear and Pressurized Components, Seville, Spain, Nov. 2001.

22. M. J. Sablik, C. Weidner, and S. W. Rubin, "Finite Element Modeling of a Magnetic Test to Determine Whether a Weld is Annealed," *J. Appl. Phys.* **91** (10), 8299 (2002).

Appendix A

M. J. SABLIK AND F. J. G. LANDGRAF
"MODELING MICROSTRUCTURAL EFFECTS ON HYSTERESIS LOOPS WITH THE SAME MAGNETIC FLUX DENSITY"
ACCEPTED BY *IEEE TRANS. MAGN.*

Modeling Microstructural Effects on Hysteresis Loops with the Same Maximum Flux Density

M. J. SABLIK, *Senior Member, IEEE,* and F. J. G. LANDGRAF

***Abstract*-- Microstructural attributes such as grain size *d* and dislocation density ζ_d affect the hysteretic magnetic properties of steels because they affect domain wall movement and pinning. In an earlier paper, a model was proposed for computing hysteresis loops based on the effect of grain size and dislocation density. In that paper, hysteresis loops were compared that all had the same maximum field H_{max}. The result was that coercivity departed from linear relationships with inverse grain size (viz. $1/d$) and $\zeta_d^{1/2}$ for large values of $1/d$ and $\zeta_d^{1/2}$. The same was true of hysteresis loss W_H, except that hysteresis loss even showed a peak, first increasing and then decreasing with increasing $1/d$ and $\zeta_d^{1/2}$. This kind of behavior had not been seen by experimenters, particularly core loss people. It was learned that the core loss experimenters compared hysteresis loops of the same maximum flux density B_{max} instead of the same H_{max}. In this paper, we use the model previously formulated to produce hysteresis loops with the same B_{max}. Indeed, the appropriate linear relationships are found. The paper also addresses effects of uniaxial anisotropy on these microstructural magnetic effects and why *two* hysteresis parameters are affected by microstructural variation.**

***Index Terms*—Hysteresis modeling, magnetic materials, microstructural effects, uniaxial *anisotropy* effects.**

Introduction

In steel, two important microstructural features that affect magnetic hysteresis are (1) grain size (i.e., average grain diameter *d*) and (2) dislocation density ζ_d. Since domain walls tend to pin at grain boundaries, the pinning of domain wall motion increases with increasing total grain boundary length as grain size *d* decreases. Since coercivity H_c reflects amount and strength of pinning, we expect H_c to increase as *d* decreases. Similarly, as dislocation density ζ_d increases, dislocations begin to get entangled, forming strong pinning centers for domain walls, so impeding domain wall motion. Thus, as ζ_d increases, so also does H_c. It has been generally established experimentally [1,2] that H_c has a linear relationship with respect to $A + B/d$ and $\zeta_d^{1/2}$, where A and B are constants. A similar relationship was also generally found for hysteresis loss W_H [3,4].

Despite all this experimental work, no one had actively modeled the effect of grain size and dislocation density on magnetic hysteresis. In two recent papers [5,6], this changed when one of the present authors (M.S.) presented a hysteresis model which was a modification of an earlier hysteresis model due to Jiles and Atherton [7] The model successfully exhibited linear behavior with $A + B/d$ and $\zeta_d^{1/2}$ for grain sizes of order larger than 15μ (where μ represents 1 micron = 10^{-6} m) and for smaller dislocation densities. In comparing hysteresis loops, the loops were all taken to the same maximum magnetic field H_{max}. The result appeared to agree with experimental results, since all the published experiments were restricted to grain sizes larger than 15μ. Core loss experimenters have now privately indicated that they can find linear results for smaller grain sizes than 15μ. However, they compare hysteresis loops taken to a constant B_{max} instead of a constant H_{max}.

It was decided therefore, in this paper, to compare modeled hysteresis loops, all taken to the same B_{max}. It was reasoned that for constant B_{max}, the remanence B_r would remain approximately constant regardless of grain size and dislocation density. Thus, hysteresis loss W_H, which is approximately B_rH_c, should show the same pattern of behavior as H_c. On the other hand, in the case where all loops are taken to a constant H_{max}, the remanence decreases with increasing inverse grain size and dislocation density, whereas the coercivity increases, causing a competition between B_r and H_c in contribution to W_H, with a maximum resulting in W_H due to the competition. We thus expect much more regular behavior for loops of constant B_{max}.

The Model

We start by referring to the basic hysteresis model of Jiles and Atherton [7], which has been modified to include the effect of stress by Sablik and Jiles [8].

In the Jiles-Atherton model, the total magnetization M is the sum of a reversible (M_{rev}) and an irreversible (M_{irr}) component. These components are given by

$$M_{rev} = c\ \left(M_a - M_{irr}\right) \tag{1}$$

$$M_{irr} = M_a - \frac{k\ \delta}{\mu_0}\frac{dM_{irr}}{dH_e} \tag{2}$$

Here, M_a is the anhysteretic magnetization, given as

$$M_a\left(H_e\right) = M_s L\left(H_e/a\ \right), \tag{3}$$

where $L(x) = \coth x - 1/x$ is the so-called Langevin function, and where H_e is the effective magnetic field in the material, i.e.

$$H_e = H + \alpha M_a\ . \tag{4}$$

The five parameters M_s, c, a, k, and α are all parameters of the material. The parameter δ is +1 or –1, depending on whether H is increasing or decreasing. Equation (2) can be reexpressed as a differential equation for dM_{irr}/dH [7,8].

Since k mathematically controls the amount of hysteresis that is present, it is proportional to the coercivity and hence has the same dependences as the coercivity. Thus, we write

$$k = \left[G_1 + G_2/d\right]\ \zeta_d^{1/2}\ \ k_o\,. \tag{5}$$

For $d = d^* = 20\mu$ and $\zeta_d = \zeta_d^* = 1 \times 10^{12}$ /m^2, we choose G_1 and G_2 so that

$$\left(G_1 + G_2/d^*\right)\ \left(\zeta_d^*\right)^{1/2} = 1\,. \tag{6}$$

A choice that satisfies this is $G_2 = 10 \times 10^{-12}$ m^2 and $G_1 = 0.5 \times 10^{-6}$ m. Other choices for G_2 and G_1 also satisfy (6). We find that various choices for G_2 and G_1 correlate with the amount of spread in the hysteresis behavior due to variation of grain size and dislocation density. Note that when d and ζ_d satisfy (6) (i.e., when $d = d^*$ and $\zeta_d = \zeta_d^*$), then $k = k_o$. The 20μ choice for grain size d^* represents a typical grain size that has been investigated. The choice of $\zeta_d^* = 1 \times 10^{12}/m^2$ represents a dislocation density quoted by papers on plastic deformation as a typical value for dislocation density in undeformed steel [4,9]. Other papers [1,10] have quoted values of the order $10^{10}/m^2$, and such values were used in [3] and [4]. Because the range of ζ_d used here is now of order $10^{12}/m^2$, the values of G_1 and G_2 are altered to accommodate this range.

Scaling constant a is proportional to domain density in the demagnetized state [8], which is determined by pinning site density, in turn proportional [7] to pinning constant k. Thus, a has the same dependence on d and ζ_d that k has, and hence

$$a = \left\{\left[G_3 + G_4/d\right]\ \zeta_d^{1/2}\right\}\ \ a_o\,. \tag{7}$$

We shall show mathematically that a is directly related to H_c. If we define G_3 and G_4 in the same way as G_1 and G_2, using (6) for $d = d^*$ and $\zeta_d = \zeta_d^*$, then we can set $G_3 = G_1$ and $G_4 = G_2$.

Results

In the following analysis, we have restricted the grain size d to 10μ, 15μ, 20μ, 25μ, and 30μ. Also, we have restricted the dislocation density ζ_d to 0.25, 0.49, 1, 2.25 and 4 $\times 10^{12}$/m^2. The two most extreme conditions occur for microstructural value sets of ($4 \times 10^{12}/m^2$, 10μ) and (0.25×10^{12} /m^2, 30μ). For hysteresis loops all of the same B_{max}, the first value set corresponds to the loop with largest H_{max}, and the second value set corresponds to the loop with smallest H_{max}. By keeping B_{max} constant for all the hysteresis loops, we end up with loops of widely varying shape and breadth, as we vary d and ζ_d. To arrive at $B_{max,}$, one increments H in smaller and smaller increments as B_{max} is neared. Here, we have B_{max}=1.03 T., $c = 0.25$, $k_0/\mu_0 = 1200$ A/m (where μ_0 is the permeability of free space), $a_0 = 1100$ A/m, $\alpha = 8.44 \times 10^{-6}$ (where α is related to λ_s via (30) in [8]), and $M_s = 1.585 \times 10^6$ A/m. Also, we have used the values for G_2 and G_1 given just below (6). The parameters are thus chosen for hard magnetic material. From the various hysteresis loops, we obtain the magnetic properties of coercive field H_c, relative permeability μ/μ_0 at field $H = H_c$, remanent flux density $B_{r,}$ and hysteresis loss W_H for each loop in the set of 25 loops corresponding to the different (ζ_d, d).

Fig. 1 is a set of plots of the different magnetic properties against square root of the dislocation density. Two things are striking. The coercive field H_c is directly proportional to the square root of the dislocation density for all values of $\zeta_d^{1/2}$, exhibiting different slopes for different grain sizes. There is no deviation from linear proportionality, as is seen for the curves when loops of the same H_{max} [5] are compared. Thus, the better way to compare hysteresis loops for different grain sizes and dislocation density is to compare loops that are all taken to the same B_{max}. The same is true for hysteresis loss W_H. The hysteresis loss is also proportional to the square root of the dislocation density in this model for all values of $\zeta_d^{1/2}$, with different slopes for different grain sizes. No maximum in W_H, appears, as was found when loops of the same H_{max} were compared [5]. The relative permeability at H_c does not exhibit linear behavior and decreases nonlinearly with increasing $\zeta_d^{1/2}$. This is similar to what was observed [5] for loops all with the same H_{max}. The remanent B_r is approximately the same for all values of ζ_d and d, as was anticipated. (See the Introduction.)

We also look at plots of the magnetic properties against inverse grain size $1/d$, as shown in Fig. 2. Here, H_c and W_H vary essentially linearly with inverse grain sizes, but with plots for different ζ_d having different intercepts. The relative permeability at H_c varies nonlinearly, decreasing with increasing $1/d$. The remanent flux density is approximately constant.

Inclusion of Uniaxial Anisotropy

One can modify the basic model, as outlined in (1)–(4), to include uniaxial anisotropy. The key modification is that [11]

$$H_e = H + \left(\alpha - \kappa_u\right) M_a\,, \tag{8}$$

where

$$\kappa_u = 2\,K_u \Big/ \left(\mu_0 M_s^2\right), \tag{9}$$

where K_u is a measure of the uniaxial anisotropy energy E_u per unit volume. Equations (1)–(3) still apply.

In this section, we study effects of uniaxial anisotropy, due perhaps to grain orientation, on magnetic hysteresis properties. For this case, $M_s = 1.585 \times 10^6$ A/m, $k_0/\mu_0 = 500$ A/m, $a_0 = 600$ A/m, $c = 0.25$ and $G_1 = 0.81 \times 10^{-6}$ and $G_2 = 3.8 \times 10^{-12}$ m^2. We treat the cases of $K_u = -1200$ J/m^3, 0, and $+1200$ J/m^3, with negative K_u corresponding to uniaxial anisotropy and positive K_u to perpendicular planar anisotropy. The interesting plots are those of magnetic properties against $\zeta_d^{1/2}$. Fig. 3 shows these plots for H_c and W_H. In particular, while the plots of H_c vs. $\zeta_d^{1/2}$ and W_H vs. $\zeta_d^{1/2}$ still exhibit linear behavior, the plots for the different grain sizes extrapolate to a value along the ordinate axis that is nonzero when K_u is nonzero. In particular, when $K_u = +1200$ J/m^3 (and with B_{max}=1.62 T for the loops), the value to which the H_c and W_H plots extrapolate is positive and nonzero, and so the H_c and W_H cannot ever be zero in this anisotropic case. $K_u=0$ lines all have intercept

$H_c=0$ and $W_H=0$. On the other hand, when K_u = -1200 J/m^3 (and with B_{max}=1.70 T for the loops), the intercept to which H_c and W_H extrapolate is negative, which actually cannot be a physical value because H_c and W_H can only be positive. The extrapolated lines also intercept the abscissa axis. All values of the abscissa $\zeta_d^{1/2}$ less than the extrapolated value at the abscissa intercept are values for which the hysteresis model is unstable and for which it cannot be used. Since uniaxial anisotropy can lead to discontinuous transitions, it is not surprising that continuous hysteresis will have some unrealizable ranges.

To see why the ordinate intercept is nonzero when K_u is nonzero, remember that the Langevin function $L(x) = coth(x) - 1/x$, and recall that the series for $coth(x)$ is such that

$$L(x) \approx x/3 - x^3/45 + 2x^5/945 \approx x/3 , \qquad (10)$$

and since $x = H_e/a$, we have that

$$M_a/M_s \approx \left[H + (\alpha - \kappa_u) M_a\right]/3a . \qquad (11)$$

If $H=H_c$, then from (11), it follows that

$$H_c \approx 3aM_a(H_c)/M_s - (\alpha - \kappa_u) M_a(H_c) \qquad (12)$$

If K_u is negative, the anisotropy term $\kappa_u M_a(H_c)$ subtracts from the K_u= 0 value of H_c. If $K_u > 0$, it adds. Also note that if pinning constant k_0 tends to zero, then M tends to M_a and since $M = 0$ at $H = H_c$, it follows that with $K_u = 0$, then

$$H_c \approx \left((3a/M_s) - \alpha\right) M_a(H_c) \approx \left((3a/M_s) - \alpha\right) M(H_c) = 0 . \qquad (13)$$

Thus, the H_c intercept is zero for $K_u = 0$; nonzero otherwise.

If one uses (7) for a, then

$$H_c \approx \left\{(3a_0/M_s)\left[G_1 + G_2/d\right]\zeta_d^{1/2} - (\alpha - \kappa_u)\right\} M_a(H_c) . \qquad (14)$$

Thus, consistent with model and experiment, it clearly is seen that H_c is linearly dependent on $\zeta_d^{1/2}$ and on [$G_1 + G_2/d$]. This behavior derives from a, and hence a must behave like k does, as asserted earlier, using a different argument.

REFERENCES

[1] J. F. Bussiere, *Mater. Eval*, Vol. 44, pp..560-567, 1986.

[2] J. Sternberk, E. Kratochilova, A. Gemperle, V. Faja, and V. Walder, *Czech. J. Phys. B*, Vol 35, pp. 1259-1267, 1985.

[3] G. Ban, P. E. Di Nunzio, S. Cicale, and T. Belgrand, *IEEE Trans. Magn.,* Vol. 34, pp. 1174-1176, 1998.

[4] J. Sternberk, E. Kratochilova, J. Hrebik, and A.Gemperle, *Phys. Status Solidi A* **,** Vol. 79, pp.523-529, 1983.

[5] M. J. Sablik, *J. Appl. Phys*., Vol..89, pp..5610-5613, 2001.

[6] M. J. Sablik, D. Stegemann, and A. Krys, *J. Appl. Phys.,* Vol. 89, pp.7254-7256, 2001.

[7] D. C. Jiles and D. L. Atherton, *J. Magn. Magn. Mater.*,Vol.61, pp.48-61, 1986.

[8] M. J. Sablik and D. C. Jiles, *IEEE Trans. Magn.*, Vol.29, 2113-2123, 1993.

[9] A. S. Keh, *Phil. Mag*., Vol.12, pp.9-30, 1965.

[10] A. H. Qureshi and L. N. Chaudhary, *J. Appl. Phys*., Vol.41, pp.1042-1043, 1970.

[11] M. J. Sablik, S. W. Rubin, L. A. Riley, D. C. Jiles, D. A. Kaminski, and S. B. Biner, *J. Appl. Phys.*, Vol.74, pp.480-488, 1993.

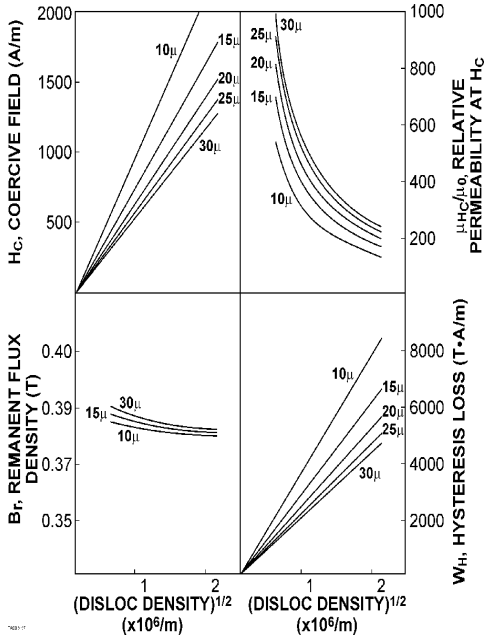

Fig. 1. Magnetic properties against square root of dislocation density ζ_d, with material parameters set as in the text. Shown are coercive field H_c, relative permeability μ/μ_0 at H_c, remanent flux density B_r, and hysteresis loss, W_H.

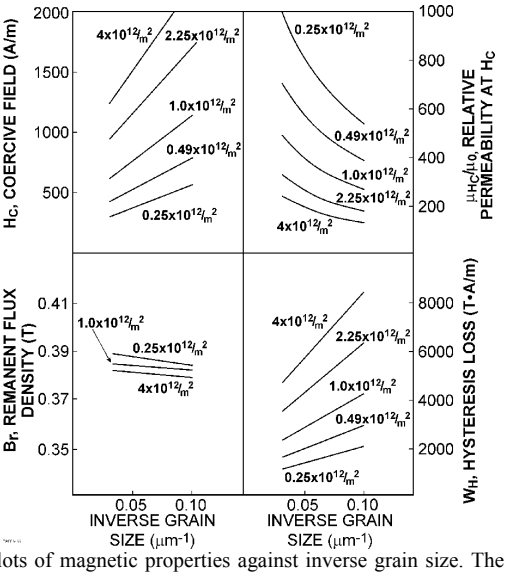

Fig. 2. Plots of magnetic properties against inverse grain size. The plots for each value of dislocation density correspond to straight lines with different intercepts, in the case of H_c and W_H. Here, parameter values are as in Fig. 1.

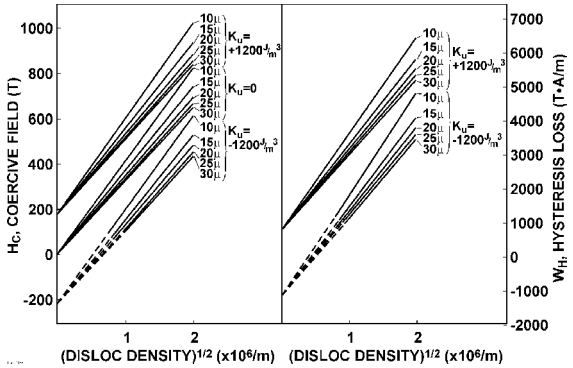

Fig. 3. Plots of (a) coercive field and (b) hysteresis loss against $\zeta_d^{1/2}$ for different grain sizes and different anisotropies K_u. The text shows why straight lines for the different anisotropies converge to different intercepts.